Progress of Theoretical Physics, Vol. 90, No. 1, July 1993

Gravitational Wave Induced by a Particle Orbiting around a Schwarzschild Black Hole

Takahiro TANAKA, Masaru SHIBATA, Misao SASAKI, Hideyuki TAGOSHI and Takashi NAKAMURA*

Department of Physics, Kyoto University, Kyoto 606-01
**Yukawa Institute for Theoretical Physics, Kyoto University Kyoto 606-01*

(Received January 18, 1993)

We have calculated gravitational waves induced by a test particle with eccentric orbits around a Schwarzschild black hole. The energy and angular momentum fluxes of gravitational waves emitted from various types of the orbits are shown. Comparing our results with those calculated by the semi-relativistic quadrupole formula, we find that, even for orbits with $r \sim 30\,M$, the amount and wave form of gravitational radiation are predominantly determined by the relativistic property, such as higher multipole contribution and curvature scattering effect of gravitational waves. We find that even in the case of circular orbits the wave form is highly deformed from a sine curve, indicating the importance of higher multipole contributions. On the other hand, the total energy flux emitted by gravitational waves is well estimated by the semi-relativistic quadrupole formula accidentally. Implications of these results to future detection of gravitational waves from a coalescing binary are also discussed.

§ 1. Introduction

Coalescence of two compact objects, such as neutron star-neutron star, neutron star-black hole and/or black hole-black hole binaries, is one of the promising sources of gravitational radiation which may be detected by future laser interferometric detectors, LIGO[1] and VIRGO.[2] Such binaries are thought to evolve in the following sequence: At first two compact objects move around each other with an eccentric orbit. As gravitational waves are emitted, both the orbital radius and the eccentricity gradually decrease. If the orbit becomes circular before the radius becomes too small, regular monochromatic gravitational waves are emitted for a sufficiently long time interval. Depending on the mass of each compact object, various phenomena will occur. For example, for almost equal mass neutron star case, when the separation of two stars becomes smaller than the radius of the last stable circular orbit, $r \sim 6M_{\rm tot}$, where $M_{\rm tot}$ is the total mass of the system, or a certain critical radius below which gravitational-radiation damping is severe, they plunge into each other and merge. Then the merging object will be a rotating black hole.

To investigate gravitational waves radiated in the above evolutionary sequence in detail, great efforts have been made by many researchers recently. As for the final coalescence phase, Nakamura, Oohara and Shibata[3)~5)] performed 3D post-Newtonian hydrodynamic simulations of coalescence of neutron stars with a wide range of initial conditions. They showed how the gravitational wave emission depends on the post-Newtonian effect, the spin of each neutron star and the plunging velocity. However their simulations should be considered as a first step to the study of real

coalescing binary neutron stars because of their approximations. As for the evolution of the orbit before merging, Lincoln and Will,[6] and Wiseman[7] performed $P^{5/2}N$ calculations with radiation damping using the point particle approximation. They found that for two equal mass particles, the final plunge orbit begins around $r=8M_{\rm tot}$ where the radial velocity becomes equal to the circular velocity. These previous investigations have revealed various important evolutionary features of two compact stars and the gravitational radiation from such objects, and the knowledge of which will definitely play a very important role in the construction of theoretical templates for LIGO and/or VIRGO. Nevertheless, there are some indications that the $P^{5/2}N$ approximation, or the post-Newtonian expansion itself, may not give a sufficiently fast converging series even at a fairly large orbital period.[8),9)] Therefore, to improve the signal-to-noise ratio in the detection of gravitational waves from a coalescing binary, and to prepare more reasonable initial conditions for future 3D relativistic numerical simulations of a coalescing binary, it is neccesary to develop a different approximation scheme which will work in a fairly (and possibly fully) relativistic regime.

As a first step toward the above goal, in this paper we consider eccentric orbits of a test particle in the Schwarzschild geometry and calculate gravitational waves induced by it. Although perturbations of a black hole by a test particle have been extensively studied,[10] the gravitational radiation from general bound orbits has not been investigated, except for circular ones. In general, compact binary systems, such as PSR1913+16, [11] PSR1534+12[12] and PSR2127+11C,[13] move with an eccentricity. Furthermore, at the final stage of coalescence the orbit necessarily deviates from a circular orbit. We then discuss the effect of radiation reaction to the orbital evolution in an approximate way.

In our approach, characteristic features of the gravitational radiation induced by the fast motion in the strong gravitational field can be investigated, although the nonlinear effect of gravity is neglected. Furthermore it has been shown that the extrapolation of the results of perturbative test particle calculations are in fairly good agreement with those of relativistic non-linear simulations: Gravitational radiation efficiency in the two black hole collision simulated by Smarr[14] coincides with the extrapolated efficiency of gravitational waves by a test particle falling into a Schwarzschild black hole.[15] The wave forms obtained in the simulation of the stellar core collapse by Stark and Piran[16] agree with those from a perturbative study of a rotating ring falling from infinity into a Schwarzschild black hole.[10] Therefore the test particle calculations are still quite meaningful and in a sense complementary to post-Newtonian calculations for the study of the gravitational radiation.

The paper is organized as follows. In § 2 we review the generalized Regge-Wheeler equation and show the formulation used in this paper. In § 3 the numerical results are shown. In § 4 we discuss implications of our results to the orbital evolution of a binary.

§ 2. Formulation

We consider gravitational waves emitted by a test particle of mass μ traveling

around a Schwarzschild black hole of mass $M(\gg\mu)$. Although many numerical studies have been done for particle orbits which are circular,[17] plunging into,[18] and scattered[19),20] by the hole, the case of bound eccentric orbits has not studied so far. Hence we first describe our method to calculate the gravitational radiation from a test particle with an eccentric orbit.

Let $\mu\varepsilon$ and μL_z be the energy and the orbital angular momentum of the particle, respectively. Throughout this paper, we set the units $c=G=M=1$. Since we can restrict the particle motion on the equatorial plane without any loss of generality, the trajectory of the particle is given by

$$\frac{dt}{d\tau}=\frac{r-2}{r}\varepsilon,$$

$$\left(\frac{dr}{d\tau}\right)^2=\varepsilon^2-1+\frac{2}{r}-\frac{L_z^2}{r^2}+\frac{2L_z^2}{r^3}\ [\equiv\gamma^2(r)],$$

$$\theta=\frac{\pi}{2},$$

$$\frac{d\varphi}{d\tau}=\frac{L_z}{r^2}. \tag{2·1}$$

For the eccentric orbit, ε and L_z are in the range,

$$\varepsilon_{\min}\leq\varepsilon\leq\varepsilon_{\max}\quad\text{for}\quad 2\sqrt{3}<L_z\leq 4,$$

$$\varepsilon_{\min}\leq\varepsilon<1\quad\text{for}\quad L_z>4, \tag{2·2}$$

where $\varepsilon_{\min}=[L_z^3+36L_z-(L_z^2-12)^{3/2}]/54L_z$ and $\varepsilon_{\max}=[L_z^3+36L_z+(L_z^2-12)^{3/2}]/54L_z$. We take the origin of time coordinate t so that the orbit $(r(t), \varphi(t))$ passes the apastron at $t=n\Delta t(n=0, \pm1, \pm2, \cdots)$, where Δt is the orbital period. For later convenience, we also introduce the functions $t(r)$ and $\varphi(r)$ which describe the part of the orbit corresponding to $0\leq t\leq\Delta t/2$. That is, $t(r_{\min})=0$ and $t(r_{\max})=\Delta t/2$ where $r_{\min}$ and $r_{\max}$ are the radii of periastron and apastron, respectively.

To evaluate gravitational waves emitted by a test particle, it is most convenient to use the generalized Regge-Wheeler equation.[21] Skipping details of its derivation, the final expression to be solved is

$$\left[\frac{d^2}{dr^{*2}}+\omega^2-\frac{r-2}{r^4}\{(\lambda+2)r-6\}\right]X_{lm\omega}(r)=S_{lm\omega}(r), \tag{2·3}$$

where $r^*=r+2\log(r/2-1)$. The boundary conditions for $X_{lm\omega}(r)$ are

$$X_{lm\omega}(r)=\begin{cases}X^{\text{in}}_{lm\omega}e^{-i\omega r^*}, & (r^*\to-\infty)\\ X^{\text{out}}_{lm\omega}e^{i\omega r^*}. & (r^*\to+\infty)\end{cases} \tag{2·4}$$

To solve Eq. (2·3), we use the Green function method. First, we construct two kinds of homogeneous solutions with the boundary conditions,

$$X^{(0)}_{\text{in}}=\begin{cases}e^{-i\omega r^*}, & r^*\to-\infty,\\ A_{\text{out}}e^{i\omega r^*}+A_{\text{in}}e^{-i\omega r^*}, & r^*\to+\infty\end{cases} \tag{2·5}$$

and

$$X^{(0)}_{\rm out}=\begin{cases} B_{\rm out}e^{i\omega r^*}+B_{\rm in}e^{-i\omega r^*}, & r^*\to-\infty, \\ e^{i\omega r^*}, & r^*\to+\infty, \end{cases} \tag{2·6}$$

where $A_{\rm out}$, $A_{\rm in}$, $B_{\rm out}$ and $B_{\rm in}$ are constants. With the help of these homogeneous solutions, the solution is given by

$$X_{lm\omega}(r)=\frac{X^{(0)}_{\rm in}\int_{r^*}^{\infty}S_{lm\omega}X^{(0)}_{\rm out}dr^*+X^{(0)}_{\rm out}\int_{-\infty}^{r^*}S_{lm\omega}X^{(0)}_{\rm in}dr^*}{2i\omega A_{\rm in}}. \tag{2·7}$$

In the limit $r\to+\infty$, the variable $X_{lm\omega}(r)$ is related to the TT-components of the metric perturbation, h_+ and $h_\times$, as

$$h_+ + ih_\times=\frac{8}{r}\int d\omega\sum_{l,m}\exp[i\omega(r^*-t)]_{-2}Y_{lm}A_{lm\omega}, \tag{2·8}$$

where

$$A_{lm\omega}=\frac{\int_{-\infty}^{+\infty}S_{lm\omega}X^{(0)}_{\rm in}dr^*}{2i\omega A_{\rm in}}. \tag{2·9}$$

and ${}_sY_{lm}(\Omega)$ is the spin weighted spherical harmonics.

The source term $S_{lm\omega}$ is constructed from a certain projection of the energy momentum tensor of the test particle, $S(t, r, \Omega)$, by expanding it in terms of the spherical harmonics and by Fourier transforming it with respect to t. In the case of a test particle coming from infinity, practically only a finite time interval of the orbit contributes to the source term. On the contrary, in the present case, the contribution from an infinite time interval must be taken into account. However, though we cannot integrate the orbit for infinite time numerically, it does not cause a true difficulty by virtue of the quasi-periodicity of the orbit:

$$r(t+\Delta t)=r(t), \quad \varphi(t+\Delta t)=\varphi(t)+\Delta\varphi, \tag{2·10}$$

where $\Delta\varphi$ is the periastron shift. Since $S(t, r, \Omega)$ mentioned above, schematically, has the form like*)

$$S(t, r, \Omega)=\mu f(r)\delta(t-t(r))\delta^{(2)}(\Omega-\Omega(r)), \tag{2·11}$$

the source term is written as

$$S_{lm\omega}(r)=\int_{-T/2}^{T/2}dt\ e^{i\omega t}\int d\Omega\ Y^*_{lm}(\Omega)S(t, r, \Omega), \tag{2·12}$$

where the time interval T is introduced to regularize the expression.

Using the quasi-periodicity (2·10), we can now integrate Eq. (2·12). Then taking the limit $T\to\infty$, we obtain

*) To be precise, $f(r)$ contains differential operators with respect to r, θ and φ, but this is not essential here.

$$S_{lm\omega}(r)=\mu\sum_n\frac{2\pi}{\Delta t}\delta(\omega-\omega_n)\tilde{S}_{lm\omega_n}(r)\,, \tag{2·13}$$

where

$$\omega_n=(2n\pi+m\varphi)/\Delta t\,,$$

$$\tilde{S}_{lm\omega_n}(r)=\int_{-\Delta t/2}^{\Delta t/2}dt\; e^{i(\omega t-m\varphi(t))}f(t)P_{lm}(\cos\theta)|_{\theta=\pi/2}\,. \tag{2·14}$$

Thus, we have only to evaluate the contribution from one period. Consequently, the Fourier spectrum of the metric perturbation has a discrete structure containing δ-functions. The explicit form of the source term is given in the Appendix.

Now we give the expressions for the energy and angular momentum fluxes emitted as gravitational waves. For the time-averaged energy flux, it is expressed as

$$\left\langle\frac{dE}{dt}\right\rangle=\lim_{T\to\infty}\frac{E}{T}$$

$$=\lim_{T\to\infty}\frac{1}{T}\sum_{l,m}\int d\omega\left(\frac{dE}{d\omega}\right)_{lm\omega}\,, \tag{2·15}$$

and the average angular momentum flux is expressed similarly. For convenience, we define the amplitude $\tilde{A}_{lm\omega}$ from $\tilde{S}_{lm\omega_n}(r)$ in the same manner as $A_{lm\omega}$ is from $S_{lm\omega_n}(r)$,

$$\tilde{A}_{lm\omega}=\frac{\int_{-\infty}^{+\infty}\tilde{S}_{lm\omega}X_{\rm in}^{(0)}dr^*}{2i\omega A_{\rm In}}\,. \tag{2·16}$$

In actual numerical calculations, we divide the integration interval in the above into three parts as $(-\infty, r^*_{\rm min})$, $[r^*_{\rm min}, r^*_{\rm max}]$, $(r^*_{\rm max}, +\infty)$. On the first interval, $S_{lm\omega}$ asymptotically behaves as $\sim e^{r^*/2}$ at $r^*\to-\infty$ and the integration can be done without any difficulty. On the second interval, $S_{lm\omega}$ diverges at both of the boundaries like $\sim 1/\gamma$. However, this apparent divergence can be eliminated by changing the independent variable r^* to t in terms of the transformation $dr^*=-(\gamma/\varepsilon)dt$. On the last interval, $S_{lm\omega}$ can be set to zero, as long as we concentrate on the out-going gravitational waves at null infinity.

In terms of $\tilde{A}_{lm\omega}$, we have

$$\lim_{T\to\infty}\frac{1}{T}\left(\frac{dE}{d\omega}\right)_{lm\omega}=\mu^2\sum_{n=-\infty}^{\infty}\frac{16\pi}{\Delta t^2}\delta(\omega-\omega_n)\omega^2|\tilde{A}_{lm\omega}|^2\,, \tag{2·17}$$

where we have used the relation,

$$\lim_{T\to\infty}\frac{2\pi}{T}(\delta(\omega-\omega_n))^2=\delta(\omega-\omega_n)\,, \tag{2·18}$$

to remove the squared δ-function. Finally, we get the convergent expression for the average energy flux as

$$\left\langle\frac{dE}{dt}\right\rangle=\mu^2\sum_{l,m,n}\frac{16\pi}{\Delta t^2}\omega_n{}^2|\tilde{A}_{lm\omega_n}|^2\,. \tag{2·19}$$

In the same way, the average angular momentum flux is expressed as

$$\left\langle \frac{dJ_z}{dt} \right\rangle = \mu^2 \sum_{l,m,n} \frac{16\pi}{\Delta t^2} m\omega_n |\tilde{A}_{lm\omega_n}|^2 . \tag{2·20}$$

As for the unaveraged (i.e., time-dependent) energy and angular momentum fluxes, we may simply use Eq. (2·8) to construct the (t, r)- and (t, φ)-components of the effective energy momentum tensor of gravitational waves. Then integrating them over the sphere of a large radius r, we obtain

$$\frac{dE}{dt} = \mu^2 \frac{16\pi}{\Delta t^2} \sum_{l,m,n,n'} \omega_n \omega_{n'} \tilde{A}_{l,m,\omega_n} \tilde{A}_{l,m,\omega_{n'}} e^{-i(\omega_n - \omega_{n'})(t-r^*)} ,$$

$$\frac{dJ_z}{dt} = \mu^2 \frac{16\pi}{\Delta t^2} \sum_{l,m,n,n'} m \frac{\omega_n + \omega_{n'}}{2} \tilde{A}_{l,m,\omega_n} \tilde{A}_{l,m,\omega_{n'}} e^{-i(\omega_n - \omega_{n'})(t-r^*)} . \tag{2·21}$$

In the following numerical calculations $\tilde{A}_{lm\omega}$ are solved for the multipoles up to $l=6$.

§ 3. Results

We have considered a wide variety of bound orbits, ranging from $L_z=3.5$ to $L_z=8$. For each L_z, we have selected ε by the following rule:

$$\varepsilon = \frac{\varepsilon_{\max} - \varepsilon_{\min}}{6} (i+0.01) + \varepsilon_{\min} , \quad i=0\sim 5 . \tag{3·1}$$

For convenience of readers who may need actual figures of the radiation efficiency for various eccentric orbits, the average energy and angular momentum fluxes emitted as gravitational waves are exhaustively listed in Table I. Recently, Cutler et al.[9] have calculated the same quantities for the case of circular orbits. They claimed that the numerical error of their calculation was less than 10^{-6}. We have also calculated one of the orbits they considered and confirmed their results to that accuracy. However, for the results listed in Table I, we did not require such high accuracy to save the computation time. Instead, we have required the relative error to be less than 10^{-4}.

From Fig. 1, it is found that if $L_z<4$, the average energy flux of gravitational waves increases as ε becomes large, but if $L_z\geq 4$, it has a peak at some ε. This can be explained as follows. For $L_z<4$, the orbital period is almost the same for all ε, while the total energy radiated per orbital period increases as ε increases. Hence the average energy flux increases monotonically. In contrast, for $L_z\geq 4$, the orbital period increases as ε increases and eventually diverges at the limit $\varepsilon\to 1$, while the increase in the total energy radiated per orbital period remains finite. As a result, the average energy flux decreases to zero in the limit $\varepsilon\to 1$.

Given the results of the energy and angular momentum fluxes $(dE/dt, dJ_z/dt)$ of the gravitational radiation for a wide variety of the orbital parameters (ε, L_z), one can estimate the effect of radiation damping on the evolution of the orbit by equating $(\mu d\varepsilon/dt, \mu dL_z/dt) = (-dE/dt, -dJ_z/dt)$, which is valid at least in the limit of small μ. For a precise treatment, we will need the precise time-dependence of $(dE/dt, dJ_z/dt)$ at each point on the orbit. However, in the small μ limit, the change in the orbital parameters is small for an orbital period and we may assume the orbit is quasi-

Table I. The list of the average energy and angular momentum fluxes emitted as gravitational waves for various bound orbits, selected according to the rule given by Eq. (3·1). The values of the fluxes are in units of μ^2. The relative error is 10^{-4} or smaller. ($l=2$) denotes the contribution from quadrupole alone and "quadrupole" denotes the values obtained in the semi-relativistic quadrupole approximation.

L_z	ε	$r_{\max}$	$r_{\min}$	Period	$dE/dt(l=2)$	$dJ_z/dt(l=2)$	dE/dt	dJ_z/dt	dE/dt_{semi}	dJ_z/dt_{semi}
‡ 3.50	.94491129	7.01738	6.98261	307.8809	3.28454E−04	6.08289E−03	3.99444E−04	7.39761E−03	3.8081E−04	7.0526E−03
3.50	.94502791	7.55443	6.44320	313.1759	3.49891E−04	6.30813E−03	4.27941E−04	7.70596E−03	4.0332E−04	7.2781E−03
3.50	.94514452	7.78929	6.20013	319.6542	3.75421E−04	6.57547E−03	4.61967E−04	8.07220E−03	4.2996E−04	7.5449E−03
3.50	.94526113	7.97281	5.99991	328.0296	4.07165E−04	6.90670E−03	5.04392E−04	8.52625E−03	4.6286E−04	7.8744E−03
3.50	.94537774	8.13013	5.81218	339.9228	4.49655E−04	7.34829E−03	5.61348E−04	9.13202E−03	5.0658E−04	8.3121E−03
3.50	.94549436	8.27092	5.61354	360.5793	5.16325E−04	8.03801E−03	6.51025E−04	1.00790E−02	5.7459E−04	8.9930E−03
3.55	.94742152	7.71109	7.64706	285.9379	2.04036E−04	4.34151E−03	2.43318E−04	5.17735E−03	2.3971E−04	5.1007E−03
3.55	.94785009	8.75781	6.70640	291.7215	2.29022E−04	4.59964E−03	2.76381E−04	5.53414E−03	2.6637E−04	5.3579E−03
3.55	.94827867	9.25278	6.31228	298.4062	2.59296E−04	4.91016E−03	3.16689E−04	5.96391E−03	2.9822E−04	5.6647E−03
3.55	.94870725	9.65699	6.00030	306.5118	2.97754E−04	5.30176E−03	3.68224E−04	6.50663E−03	3.3807E−04	6.0483E−03
3.55	.94913583	10.0164	5.71761	317.2197	3.50688E−04	5.83668E−03	4.39633E−04	7.24894E−03	3.9201E−04	6.5679E−03
3.55	.94956441	10.3488	5.42831	334.3592	4.37142E−04	6.70298E−03	5.57126E−04	8.45289E−03	4.7846E−04	7.4014E−03
3.60	.94964718	8.28967	8.19788	285.0710	1.42231E−04	3.36615E−03	1.67367E−04	3.96101E−03	1.6813E−04	3.9791E−03
3.60	.95049409	9.86691	6.90607	293.2402	1.67368E−04	3.62003E−03	2.00496E−04	4.31591E−03	1.9531E−04	4.2309E−03
3.60	.95134100	10.6670	6.39449	302.3480	1.98005E−04	3.92592E−03	2.41283E−04	4.74448E−03	2.2772E−04	4.5296E−03
3.60	.95218791	11.3488	6.00109	312.8414	2.37309E−04	4.31426E−03	2.94133E−04	5.28956E−03	2.6833E−04	4.9035E−03
3.60	.95303482	11.9780	5.65309	325.7221	2.92268E−04	4.85205E−03	3.68786E−04	6.04558E−03	3.2371E−04	5.4139E−03
3.60	.95388173	12.5799	5.30501	344.2115	3.84469E−04	5.74581E−03	4.95372E−04	7.30370E−03	4.1403E−04	6.2505E−03
3.65	.95166482	8.82021	8.70032	290.2356	1.04649E−04	2.71289E−03	1.21865E−04	3.15919E−03	1.2409E−04	3.2169E−03
3.65	.95301047	10.9809	7.07547	302.2702	1.28785E−04	2.94968E−03	1.53566E−04	3.49465E−03	1.5048E−04	3.4504E−03
3.65	.95435613	12.1555	6.46253	315.6229	1.58094E−04	3.23211E−03	1.92613E−04	3.89630E−03	1.8159E−04	3.7223E−03
3.65	.95570178	13.2021	6.00224	330.7485	1.95684E−04	3.58923E−03	2.43387E−04	4.40549E−03	2.2024E−04	4.0586E−03
3.65	.95704744	14.2077	5.60283	348.6001	2.48543E−04	4.08625E−03	3.15750E−04	5.11510E−03	2.7279E−04	4.5173E−03
3.65	.95839309	15.2079	5.21042	372.1008	3.38756E−04	4.92861E−03	4.40919E−04	6.31797E−03	3.5923E−04	5.2813E−03

(continued)

L_z	ε	$r_{\max}$	$r_{\min}$	Period	$dE/dt(l=2)$	$dJ_z/dt(l=2)$	dE/dt	dJ_z/dt	$dE/dt_{\rm semi}$	$dJ_z/dt_{\rm semi}$
3.70	.95351603	9.32489	9.17594	298.2261	7.96058E−05	2.23914E−03	9.19033E−05	2.58502E−03	9.4532E−05	2.6589E−03
3.70	.95542656	12.1391	7.22589	315.6783	1.02255E−04	2.45330E−03	1.21564E−04	2.89334E−03	1.1952E−04	2.8687E−03
3.70	.95733709	13.7803	6.52177	335.3793	1.29381E−04	2.70244E−03	1.57765E−04	3.25451E−03	1.4836E−04	3.1039E−03
3.70	.95924762	15.3157	6.00373	357.9513	1.63772E−04	3.01199E−03	2.04493E−04	3.70510E−03	1.8347E−04	3.3866E−03
3.70	.96115814	16.8607	5.56143	384.5209	2.11857E−04	3.44042E−03	2.70929E−04	4.32923E−03	2.3049E−04	3.7674E−03
3.70	.96306867	18.4701	5.13328	418.0705	2.94492E−04	4.17693E−03	3.86906E−04	5.39943E−03	3.0772E−04	4.4097E−03
3.75	.95522814	9.81423	9.63499	307.8914	6.19852E−05	1.87915E−03	7.10308E−05	2.15335E−03	7.3634E−05	2.2323E−03
3.75	.95776017	13.3664	7.36283	332.5237	8.29381E−05	2.06820E−03	9.84035E−05	2.43094E−03	9.6942E−05	2.4158E−03
3.75	.96029220	15.5954	6.57486	361.2507	1.07401E−04	2.27834E−03	1.31149E−04	2.74362E−03	1.2293E−04	2.6087E−03
3.75	.96282423	17.7969	6.00553	395.2490	1.37634E−04	2.52962E−03	1.72548E−04	3.12047E−03	1.5348E−04	2.8276E−03
3.75	.96535626	20.1356	5.52625	436.3897	1.79024E−04	2.86990E−03	2.30395E−04	3.63102E−03	1.9312E−04	3.1130E−03
3.75	.96788829	22.7153	5.06816	488.5968	2.49688E−04	3.45985E−03	3.30905E−04	4.50891E−03	2.5720E−04	3.5996E−03
3.80	.95682084	10.2942	10.0832	318.7079	4.91211E−05	1.59690E−03	5.59235E−05	1.81801E−03	5.8332E−05	1.8963E−03
3.80	.96002406	14.6843	7.48951	352.5842	6.83032E−05	1.75991E−03	8.09354E−05	2.06339E−03	7.9812E−05	2.0527E−03
3.80	.96322728	17.6600	6.62334	393.8983	8.98322E−05	1.92758E−03	1.09884E−04	2.32258E−03	1.0263E−04	2.1997E−03
3.80	.96643050	20.7864	6.00764	445.3008	1.15262E−04	2.11335E−03	1.45080E−04	2.61519E−03	1.2795E−04	2.3484E−03
3.80	.96963372	24.3323	5.49575	510.9633	1.48550E−04	2.35167E−03	1.92336E−04	2.99163E−03	1.5891E−04	2.5270E−03
3.80	.97283694	28.5423	5.01192	598.4879	2.03798E−04	2.76520E−03	2.72302E−04	3.63179E−03	2.0702E−04	2.8358E−03
3.85	.95830915	10.7685	10.5242	330.4016	3.94724E−05	1.37053E−03	4.46780E−05	1.55125E−03	4.6835E−05	1.6261E−03
3.85	.96222788	16.1135	7.60796	375.9778	5.68817E−05	1.50740E−03	6.73481E−05	1.76405E−03	6.6439E−05	1.7552E−03
3.85	.96614662	20.0479	6.66817	434.7531	7.53316E−05	1.63055E−03	9.23210E−05	1.96667E−03	8.5910E−05	1.8544E−03
3.85	.97006535	24.4881	6.01001	512.9720	9.55409E−05	1.74615E−03	1.20731E−04	2.16798E−03	1.0559E−04	1.9289E−03
3.85	.97398409	29.9515	5.46894	621.4014	1.19754E−04	1.87374E−03	1.55956E−04	2.39646E−03	1.2705E−04	1.9948E−03
3.85	.97790283	37.1151	4.96255	780.6256	1.57131E−04	2.09221E−03	2.11580E−04	2.76838E−03	1.5743E−04	2.1155E−03

(continued)

L_z	ε	$r_{\max}$	$r_{\min}$	Period	$dE/dt(l=2)$	$dJ_z/dt(l=2)$	dE/dt	dJ_z/dt	dE/dt_{semi}	dJ_z/dt_{semi}
3.90	.95970501	11.2397	10.9605	342.8154	3.20830E−05	1.18581E−03	3.61241E−05	1.33515E−03	3.8021E−05	1.4052E−03
3.90	.96437927	17.6771	7.71961	403.0459	4.77575E−05	1.29689E−03	5.65201E−05	1.51564E−03	5.5756E−05	1.5073E−03
3.90	.96905352	22.8566	6.71005	486.1237	6.30699E−05	1.37450E−03	7.74475E−05	1.66001E−03	7.1795E−05	1.5578E−03
3.90	.97372778	29.2176	6.01265	606.7198	7.78250E−05	1.41752E−03	9.87251E−05	1.76592E−03	8.5634E−05	1.5567E−03
3.90	.97840204	37.9123	5.44513	794.4836	9.24289E−05	1.43085E−03	1.21047E−04	1.83958E−03	9.7270E−05	1.5093E−03
3.90	.98307629	51.0656	4.91870	1118.553	1.10718E−04	1.44961E−03	1.50192E−04	1.93173E−03	1.0943E−04	1.4454E−03
3.95	.96101817	11.7095	11.3936	355.8537	2.63284E−05	1.03299E−03	2.95035E−05	1.15753E−03	3.1155E−05	1.2223E−03
3.95	.96648438	19.4013	7.82549	434.3251	4.03290E−05	1.11891E−03	4.77201E−05	1.30639E−03	4.7061E−05	1.2979E−03
3.95	.97195059	26.2213	6.74946	551.5628	5.25094E−05	1.15075E−03	6.46112E−05	1.39189E−03	5.9664E−05	1.2997E−03
3.95	.97741681	35.4985	6.01552	741.8016	6.17489E−05	1.12102E−03	7.86295E−05	1.40128E−03	6.7647E−05	1.2238E−03
3.95	.98288302	50.1199	5.42383	1091.553	6.67072E−05	1.02285E−03	8.78383E−05	1.32168E−03	6.9636E−05	1.0691E−03
3.95	.98834923	77.9115	4.87938	1886.862	6.64485E−05	8.57033E−04	9.07850E−05	1.14980E−03	6.4808E−05	8.4289E−04
4.00	.96225674	12.1793	11.8249	369.4552	2.17850E−05	9.05117E−04	2.43054E−05	1.00981E−03	2.5736E−05	1.0692E−03
4.00	.96854833	21.3176	7.92637	470.5615	3.41855E−05	9.66694E−04	4.04512E−05	1.12795E−03	3.9872E−05	1.1192E−03
4.00	.97483992	30.3370	6.78677	636.5915	4.32908E−05	9.53267E−04	5.33781E−05	1.15491E−03	4.9099E−05	1.0729E−03
4.00	.98113151	44.2718	6.01862	947.9636	4.71267E−05	8.53069E−04	6.02348E−05	1.06991E−03	5.1404E−05	9.2591E−04
4.00	.98742310	71.2865	5.40465	1683.497	4.30437E−05	6.54468E−04	5.69805E−05	8.49795E−04	4.4576E−05	6.7785E−04
4.00	.99371469	151.274	4.84385	4604.476	2.76037E−05	3.51394E−04	3.79813E−05	4.74524E−04	2.6585E−05	3.4101E−04
4.25	.96753590	14.4695	14.0624	444.7804	9.27231E−06	4.99257E−04	1.01641E−05	5.47262E−04	1.0846E−05	5.8399E−04
4.25	.97294748	25.0333	9.63148	569.4436	1.30791E−05	4.97254E−04	1.50169E−05	5.63998E−04	1.5353E−05	5.7737E−04
4.25	.97835907	35.4994	8.37764	774.8033	1.49276E−05	4.54048E−04	1.76918E−05	5.29584E−04	1.7368E−05	5.2065E−04
4.25	.98377065	51.6864	7.56469	1161.178	1.43632E−05	3.69941E−04	1.74770E−05	4.42124E−04	1.6461E−05	4.1734E−04
4.25	.98918224	83.0834	6.95425	2076.895	1.11012E−05	2.49710E−04	1.38314E−05	3.05138E−04	1.2478E−05	2.7627E−04
4.25	.99459382	176.069	6.46039	5725.557	5.42122E−06	1.08580E−04	6.90808E−06	1.35505E−04	5.9618E−06	1.1751E−04

(continued)

L_z	ε	$r_{\max}$	$r_{\min}$	Period	$dE/dt(l=2)$	$dJ_z/dt(l=2)$	dE/dt	dJ_z/dt	$dE/dt_{\rm semi}$	$dJ_z/dt_{\rm semi}$
4.50	.97167901	16.8224	16.3587	531.4326	4.40528E−06	2.97483E−04	4.76701E−06	3.21904E−04	5.0986E−06	3.4429E−04
4.50	.97639996	28.8927	11.3346	683.2509	5.88253E−06	2.85936E−04	6.61624E−06	3.18158E−04	6.8859E−06	3.3055E−04
4.50	.98112092	40.8761	9.92934	933.7932	6.40704E−06	2.52215E−04	7.39905E−06	2.87090E−04	7.4978E−06	2.8998E−04
4.50	.98584187	59.4215	9.02752	1405.970	5.88444E−06	1.98341E−04	6.94428E−06	2.30227E−04	6.8489E−06	2.2613E−04
4.50	.99056282	95.4041	8.35855	2526.753	4.32917E−06	1.28925E−04	5.20782E−06	1.52295E−04	4.9959E−06	1.4545E−04
4.50	.99528377	201.986	7.82539	6998.570	2.00206E−06	5.37857E−05	2.45205E−06	6.45733E−05	2.2896E−06	5.9980E−05
4.75	.97502103	19.2651	18.7414	629.2391	2.25723E−06	1.86864E−04	2.41831E−06	2.00196E−04	2.5857E−06	2.1405E−04
4.75	.97918488	32.9226	13.0812	811.6130	2.91459E−06	1.75744E−04	3.22793E−06	1.92782E−04	3.3908E−06	2.0178E−04
4.75	.98334874	46.4991	11.5068	1112.913	3.08899E−06	1.51914E−04	3.49979E−06	1.69884E−04	3.6095E−06	1.7415E−04
4.75	.98751259	67.5184	10.5010	1681.337	2.76538E−06	1.17150E−04	3.19187E−06	1.33188E−04	3.2303E−06	1.3373E−04
4.75	.99167645	108.309	9.75850	3031.863	1.98356E−06	7.46859E−05	2.32726E−06	8.61636E−05	2.3102E−06	8.4749E−05
4.75	.99584030	229.146	9.16975	8425.097	8.93821E−07	3.05522E−05	1.06484E−06	3.57243E−05	1.0381E−06	3.4437E−05
5.00	.97777106	21.8111	21.2241	738.5136	1.22435E−06	1.22126E−04	1.30129E−06	1.29798E−04	1.3891E−06	1.3856E−04
5.00	.98147650	37.1369	14.8896	954.9593	1.54551E−06	1.13182E−04	1.69104E−06	1.22780E−04	1.7848E−06	1.2897E−04
5.00	.98518194	52.3849	13.1334	1312.828	1.60878E−06	9.65334E−05	1.79579E−06	1.06486E−04	1.8712E−06	1.1008E−04
5.00	.98888738	75.9987	12.0142	1988.467	1.41679E−06	7.35099E−05	1.60747E−06	8.22564E−05	1.6523E−06	8.3692E−05
5.00	.99259282	121.831	11.1898	3594.843	1.00026E−06	4.62981E−05	1.15127E−06	5.24660E−05	1.1669E−06	5.2535E−05
5.00	.99629826	257.614	10.5379	10014.09	4.43738E−07	1.87169E−05	5.17601E−07	2.14563E−05	5.1815E−07	2.1155E−05
5.50	.98201454	27.2392	26.5160	993.3970	4.09479E−07	5.70212E−05	4.30010E−07	5.98796E−05	4.5683E−07	6.3613E−05
5.50	.98501262	46.1479	18.7252	1289.232	5.02445E−07	5.18753E−05	5.39974E−07	5.53578E−05	5.7150E−07	5.8241E−05
5.50	.98801069	64.9806	16.5730	1778.882	5.11517E−07	4.35132E−05	5.58584E−07	4.70499E−05	5.8752E−07	4.9007E−05
5.50	.99100877	94.1563	15.2047	2704.264	4.41587E−07	3.26270E−05	4.88550E−07	3.56779E−05	5.1012E−07	3.6783E−05
5.50	.99400684	150.794	14.1993	4906.609	3.05959E−07	2.02518E−05	3.42404E−07	2.23661E−05	3.5476E−07	2.2819E−05
5.50	.99700492	318.607	13.4060	13716.10	1.33248E−07	8.07393E−06	1.50726E−07	8.99732E−06	1.5524E−07	9.0885E−06

(continued)

L_z	ε	$r_{\max}$	$r_{\min}$	Period	$dE/dt(l=2)$	$dJ_z/dt(l=2)$	dE/dt	dJ_z/dt	dE/dt_{semi}	dJ_z/dt_{semi}
6.00	.98511463	33.1386	32.2664	1300.371	1.55720E−07	2.91032E−05	1.62129E−07	3.03006E−05	1.7131E−07	3.2016E−05
6.00	.98759594	55.9616	22.8793	1691.832	1.87910E−07	2.61858E−05	1.99395E−07	2.76224E−05	2.1076E−07	2.9009E−05
6.00	.99007725	78.7070	20.2909	2340.218	1.88824E−07	2.17482E−05	2.03029E−07	2.31896E−05	2.1404E−07	2.4193E−05
6.00	.99255856	113.951	18.6473	3566.455	1.61133E−07	1.61592E−05	1.75133E−07	1.73894E−05	1.8392E−07	1.8015E−05
6.00	.99503986	182.380	17.4409	6486.838	1.10439E−07	9.94502E−06	1.21180E−07	1.07890E−05	1.2671E−07	1.1095E−05
6.00	.99752117	385.137	16.4900	18176.71	4.75966E−08	3.93315E−06	5.26918E−08	4.29828E−06	5.4969E−08	4.3899E−06
6.50	.98745903	39.5236	38.4896	1664.013	6.52515E−08	1.58864E−05	6.75017E−08	1.64341E−05	7.0957E−08	1.7275E−05
6.50	.98954954	66.5948	27.3674	2168.837	7.78965E−08	1.41910E−05	8.18797E−08	1.48417E−05	8.6302E−08	1.5540E−05
† 6.50	.99164005	93.5847	24.3040	3005.426	7.76184E−08	1.17099E−05	8.25017E−08	1.23578E−05	8.6914E−08	1.2881E−05
6.50	.99373056	135.412	22.3602	4588.409	6.57422E−08	8.64874E−06	7.05184E−08	9.19792E−06	7.4158E−08	9.5400E−06
6.50	.99582107	216.628	20.9343	8360.353	4.47458E−08	5.29317E−06	4.83838E−08	5.66755E−06	5.0766E−08	5.8468E−06
6.50	.99791158	457.285	19.8111	23466.82	1.91548E−08	2.08242E−06	2.08686E−08	2.24340E−06	2.1892E−08	2.3027E−06
7.00	.98928000	46.4017	45.1931	2088.984	2.95306E−08	9.14665E−06	3.03980E−08	9.41524E−06	3.1803E−08	9.8505E−06
7.00	.99106696	78.0565	32.1974	2726.406	3.49944E−08	8.12965E−06	3.65171E−08	8.44666E−06	3.8361E−08	8.8154E−06
7.00	.99285393	109.624	28.6206	3783.156	3.46679E−08	6.67799E−06	3.65237E−08	6.99197E−06	3.8398E−08	7.2744E−06
7.00	.99464089	158.553	26.3521	5783.516	2.92127E−08	4.91172E−06	3.10184E−08	5.17661E−06	3.2595E−08	5.3660E−06
7.00	.99642785	253.561	24.6887	10551.87	1.97876E−08	2.99432E−06	2.11563E−08	3.17411E−06	2.2210E−08	3.2769E−06
7.00	.99821482	535.094	23.3789	29656.69	8.43240E−09	1.17372E−06	9.07420E−09	1.25071E−06	9.5370E−09	1.2863E−06
7.50	.99072521	53.7772	52.3812	2579.970	1.42357E−08	5.50169E−06	1.45966E−08	5.64112E−06	1.5207E−08	5.8771E−06
7.50	.99227126	90.3519	37.3735	3370.721	1.67810E−08	4.87221E−06	1.74109E−08	5.03601E−06	1.8227E−08	5.2388E−06
7.50	.99381732	126.834	33.2453	4682.075	1.65553E−08	3.98905E−06	1.73198E−08	4.15068E−06	1.8162E−08	4.3083E−06
7.50	.99536337	183.382	30.6277	7165.156	1.38986E−08	2.92504E−06	1.46397E−08	3.06094E−06	1.5357E−08	3.1685E−06
7.50	.99690943	293.191	28.7090	13086.05	9.38176E−09	1.77807E−06	9.94158E−09	1.87003E−06	1.0427E−08	1.9296E−06
7.50	.99845549	618.590	27.1985	36816.21	3.98450E−09	6.95075E−07	4.24614E−09	7.34334E−07	4.4631E−09	7.5556E−07
8.00	.99189286	61.6528	60.0564	3141.675	7.23631E−09	3.43312E−06	7.39637E−09	3.50903E−06	7.6772E−09	3.6422E−06
8.00	.99324427	103.484	42.8986	4107.974	8.49697E−09	3.03204E−06	8.77520E−09	3.12093E−06	9.1571E−09	3.2366E−06
8.00	.99459569	145.216	38.1806	5710.851	8.35677E−09	2.47629E−06	8.69343E−09	2.56376E−06	9.0914E−09	2.6547E−06
8.00	.99594710	209.906	35.1899	8746.699	6.99652E−09	1.81161E−06	7.32201E−09	1.88497E−06	7.6640E−09	1.9477E−06
8.00	.99729852	335.527	32.9980	15987.48	4.71043E−09	1.09884E−06	4.95567E−09	1.14836E−06	5.1897E−09	1.1836E−06
8.00	.99864993	707.790	31.2729	45015.11	1.99548E−09	4.28662E−07	2.10982E−09	4.49757E−07	2.2155E−09	4.6255E−07

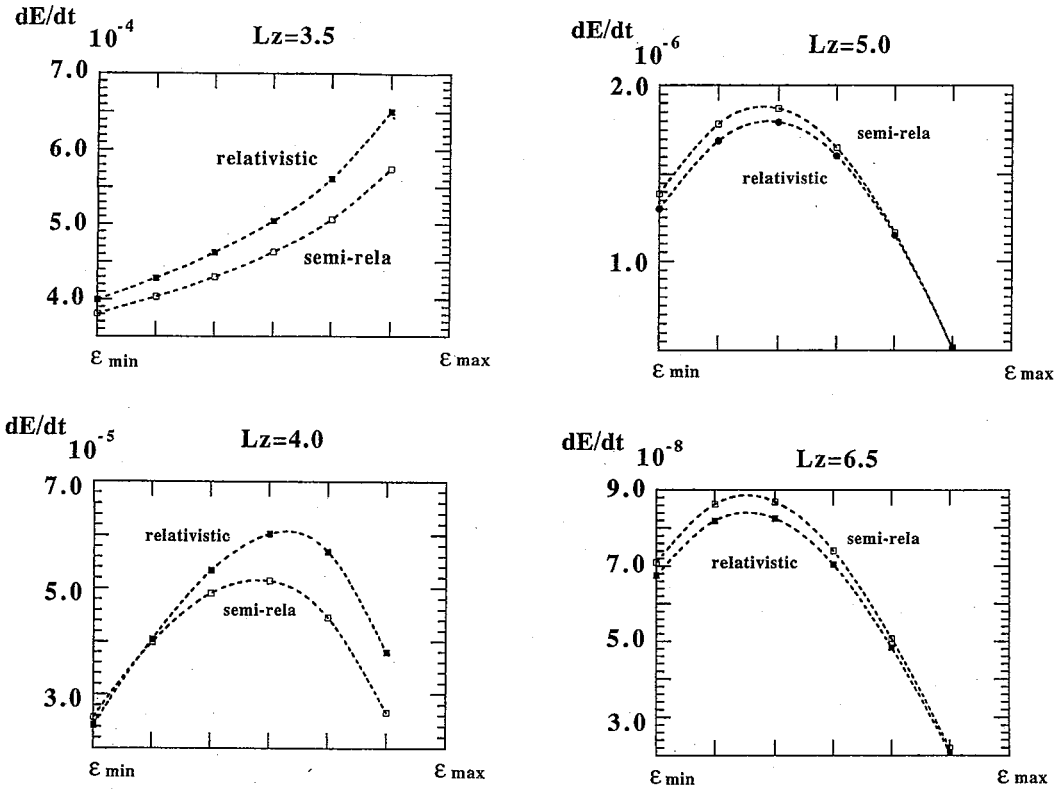

Fig. 1. Comparison of the average energy fluxes calculated in the fully relativistic and semi-relativistic manners, for several typical values of the angular momentum of the test particle; L_z =(3.5, 4.0, 5.0, 6.5). The horizontal axis is the energy of the test particle.

periodic for many periods. Therefore we may replace $(dE/dt, dJ_z/dt)$ by their time averages and consider the evolutionary path of the orbit on the (ε, L_z)-plane. In this case, since only the direction of the vector $(d\varepsilon/dt, dL_z/dt)$ is relevant but not its magnitude, we can easily construct such a path on the (ε, L_z)-plane.

Figure 2 shows several evolutionary paths constructed in this way from our numerical results. We plot these paths with respect to the energy normalized to the difference of the maximal and the minimal possible energies, i.e., $(\varepsilon-\varepsilon_{\min})/(\varepsilon_{\max}-\varepsilon_{\min})$, we find the relative deviation from the quasi-circular path begins to increase as L_z goes down below 4. Although our results are valid only in the limit $\mu \ll 1$, if qualitative features are essentially correct even for $\mu=O(1)$ (note that μ can be naturally identified as the reduced mass of the system, in which case $\mu \leq 1/4$), the above result may be important to constrain physically reasonable initial conditions to be used for 3D relativistic simulations of a coalescing binary.

To see general relativistic effects of the particle motion, we have compared our results with the calculation using the quadrupole formula. In the case of circular orbits, an orbit can be completely specified by its period seen from the null infinity. Therefore, we can directly compare the results with those obtained using the quadrupole formula, and we know that the quadrupole formula gives a fairly good

estimate of the energy and angular momentum fluxes for circular orbits,[10] though we will see below that it happens only by chance.

In contrast with the case of circular orbits, in the present case, two parameters are necessary to determine the orbit. Hence, if we want to make comparison with the quadrupole formula, we need to specify one additional parameter other than the orbital period. However we do not have such natural parametrizations. Hence, provisionally we have compared our results with those obtained by the semi-relativistic approximation proposed by Ruffini and Sasaki.[22] Specifically, the particle trajectory is determined by the equations of motion in the Schwarzschild spacetime but the energy and angular momentum losses are evaluated as if the orbit were in flat spacetime. Further, for simplicity, we have taken up only the quadrupole contribution to the gravitational radiation in the semi-relativistic approximation. The idea of this approximation is similar to the method adopted by Kidder et al.[8] Then we have a natural correspondence between the orbit in the relativistic and semi-relativistic treatments, because the trajectory is completely determined by ε and L_z in both cases.

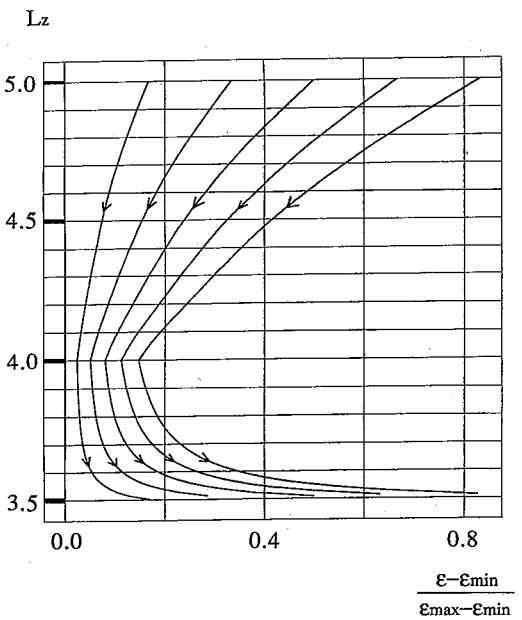

Fig. 2. Expected trajectories of the orbits in the $((\varepsilon-\varepsilon_{\min})/(\varepsilon_{\max}-\varepsilon_{\min}), L_z)$-plane, assuming the effect of gravitational-radiation damping is small during each orbital period. The energy of the particle normalized to the difference of the maximally and minimally allowed values of it.

However, in addition, we need to specify the identification between the points in Schwarzschild spacetime and those in flat spacetime when we apply the quadrupole formula. Here we have identified the Schwarzschild spherical coordinates with the spherical coordinates in flat spacetime. The reason is that 1) in the limit of the circular orbit, the proper length of the orbit ($=2\pi r$) in both coordinates agrees with each other, and 2) the energy flux at null infinity is measured in units of the Schwarzschild time t, which properly takes care of the gravitational redshift effect. In this identification, the semi-relativistic approximation gives the same value with the quadrupole formula in the limit of circular orbit.

In Fig. 1, we show the average energy flux calculated in both ways, i.e., in relativistic and semi-relativistic manners, for $L_z=3.5$, 4.0, 5.0 and 6.5. Note that smaller ε corresponds to more circular orbit. We find the semi-relativistic quadrupole approximation is fairly good even in the case of eccentric orbits, as in the case of circular orbits. The relative errors of the semi-relativistic approximation in the energy and angular momentum fluxes for various orbits are shown in Fig. 5. We see that for $r_{\min}\gtrsim 10$ the relative error is less than 8 %.

We show the wave forms in Fig. 3(a) and the corresponding energy fluxes as

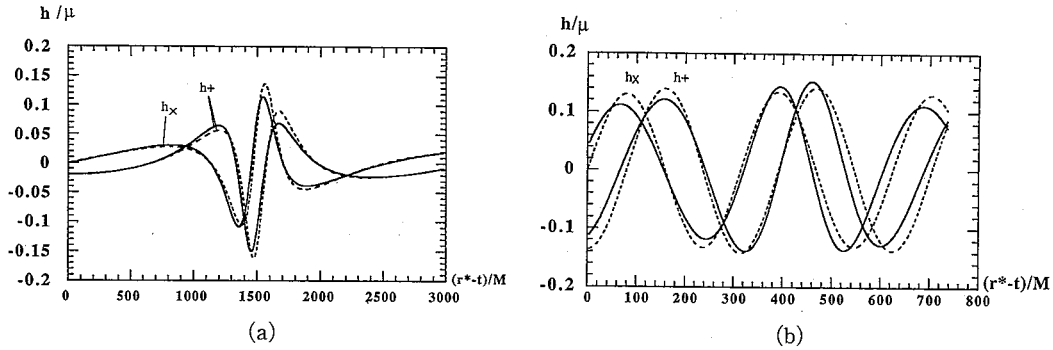

Fig. 3. Wave patterns observed from the direction of $(\theta, \varphi)=(\pi/4, 0)$ for the orbital parameters indicated in Table I (a) by †, i.e., $(L_z, \varepsilon)=(6.50, .9916401)$, and (b) by ‡, i.e., $(L_z, \varepsilon)=(3.50, .9449113)$. The real lines are the wave forms in the fully relativistic treatment. The dotted lines are those in the semi-relativistic approximation.

functions of time in Fig.4, for $(L_z, \varepsilon)=(6.5, 0.97771)$, for which $r_{\min}=24.3$. The wave form obtained from semi-relativistic approximation is shown as before and they also coincide well. Hence the semi-relativistic method seems to be a fairly good approximation to the fully general relativistic calculation of gravitational waves. This also suggests that the method adopted by Kidder et al.[8] gives a fairly good estimate of the last stable orbit.

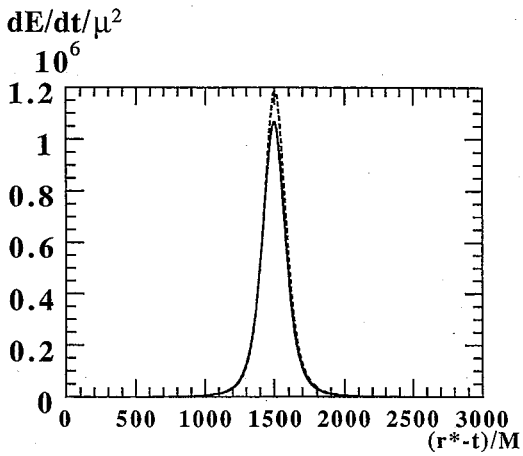

Fig. 4. The energy flux as a function of time for the same orbital parameters of Fig. 3(a), i.e., indicated by † in Table I. As before the real line is the calculated result, while the dotted line is the result of the semi-relativistic approximation.

In Fig. 3(b), we show the wave form for $(L_z, \varepsilon)=(5.0, 0.94491)$. In this case the orbit of the test particle is almost circular; $r\approx 21$. However, the wave form is substantially deformed from a sine curve which would be expected if it were dominated by the quadrupole. This means that contributions of higher multipoles to the wave form are important; $\gtrsim 30\%$ for $r\lesssim 10$, even for circular orbits.[7] This results seem to contradict with the fact that the energy and angular momentum fluxes calculated in both relativistic and semi-relativistic method coincide. The reason is as follows. In semi-relativistic calculation, we ignore two effects, 1) back scattering of waves by space-time curvature, 2) the contribution of the higher multipoles ($l\geq 3$). To see these effects, we show the following two figures; in Fig. 6 the relative error of the energy flux calculated using the semi-relativistic formula to those by the relativistic method, but only the contribution of the quadrupole component is shown and in Fig. 7 the ratio of quadrupole contribution to the total energy flux, $\dot{E}^{l=2}/\dot{E}^{\text{total}}$. From Fig. 6, we can estimate the curvature scattering effects because in semi-relativistic formula the curvature

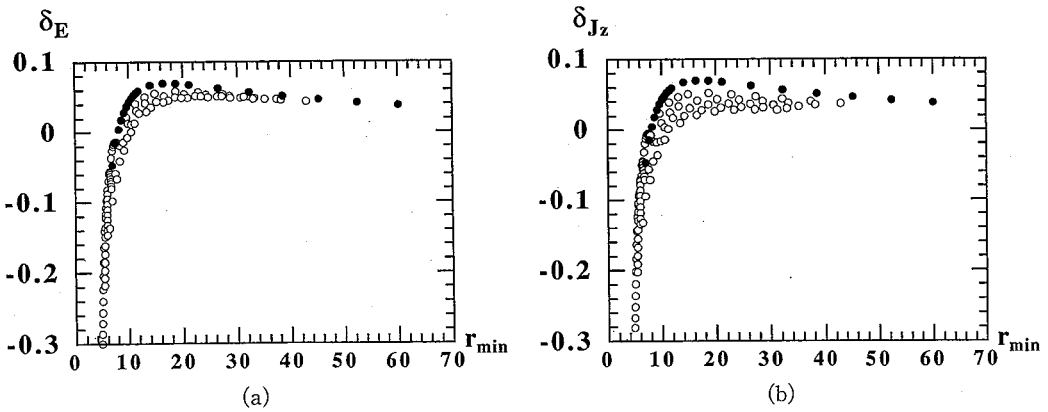

Fig. 5. Plot of relative errors in the semi-relativistic estimation to the fully relativistic calculation of (a) the average energy flux and (b) the average angular momentum flux, against the periastron radius r_{min}. The vertical coordinate is $\delta_Q=(\dot{Q}_{semi\text{-}rel}-\dot{Q}_{rel})/\dot{Q}_{rel}$, where $Q=E$ or J_z. All orbits in Table I are plotted. The closed circles denote the cases of almost circular orbits.

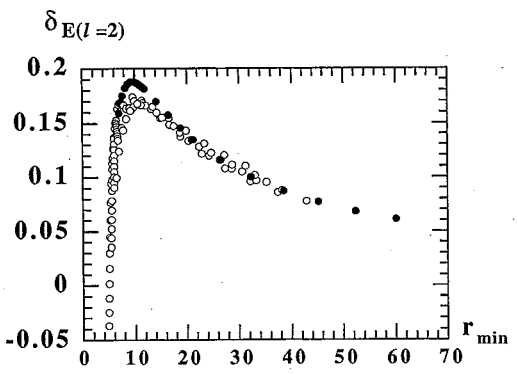

Fig. 6. Same plot as Fig. 5(a) but compared with the energy flux where only the quadrupole contribution is accounted.

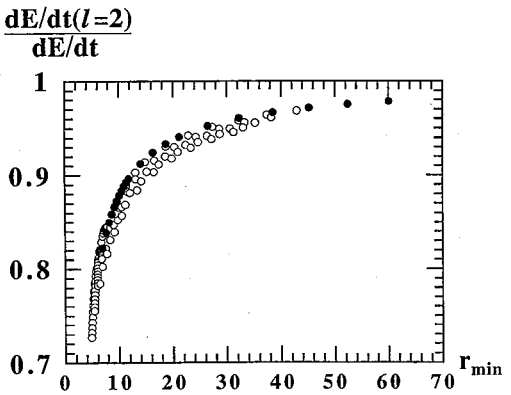

Fig. 7. Plot of the ratio of the quadrupole component to the total energy flux. The closed circles are the same as above mentioned.

scattering of gravitational waves is neglected in contrast with the relativistic calculation. We find that the relative error is as large as 10 %(20 %) *in excess* even at $r_{min}\sim30(10)$ almost independent of the orbital eccentricity. On the other hand, from Fig. 7 we find that the contribution of multipoles other than the quadrupole part to the total energy is as large as 5 % even at $r_{min}\sim30$ and 12 % at $r_{min}\sim10$ also almost independent of the orbital eccentricity.

Thus we can say that the cancellation of these two effects happens to reduce the relative error, although each of them is large even at $r_{min}\sim30$. This explains why the quadrupole formula for the circular orbit and the semi-relativistic formula for the eccentric orbit gives a good estimate of the energy and the angular momentum fluxes. Hence if the observation of gravitational waves is in operation in the future, we may directly detect the general relativistic effect on the wave form of the gravitational radiation produced in the final phase of coalescence.

It should be also mentioned that the dependence of $\delta_E{}^{l=2}$ and $\dot{E}_{l=2}/\dot{E}_{\rm total}-1$ on $r_{\rm min}$ are almost independent of the orbital eccentricity. In particular, $\dot{E}_{l=2}/\dot{E}_{\rm total}-1\propto r_{\rm min}^{-1}$.

§ 4. Discussion

We have calculated the gravitational waves induced by a test particle with eccentric orbits in the Schwarzschild spacetime. Comparing our results with the semi-relativistic formula, we have found that the curvature scattering effect and the higher multipole contributions of gravitational waves are important even in the region far away from the event horizon. We have also found that the dependence of these two effects on $r_{\rm min}$ is almost independent of the orbital eccentricity. This suggests that one may improve the semi-relativistic method by adding the phenomenological correction terms as done by Kidder et al.[8] (or specifying empirical identification between the Schwarzschild and semi-relativistic radial coordinates.)

Since the semi-relativistic approximation or a certain extension of it can be dealt with in a more analytical manner than the fully relativistic perturbation method, and may be quite useful, it is worth while to discuss here the merits and demerits of the semi-relativistic approximation in comparison with those of the post-Newtonian expansion. The merits of the post-Newtonian expansion is that its applicability is not constrained by the magnitude of μ, while the semi-relativistic approximation is valid, if at all, only in the limit $\mu\ll 1$. The demerits of the post-Newtonian expansion seem to be the following four points:

1) The orbit is not determined in a sufficiently relativistic manner.
2) The higher order multipole contributions to the gravitational radiation can be evaluated, but only the quadrupole contribution to the radiation reaction force can be included, at least at presently available level.
3) The gravitational redshift of gravitational waves is not sufficiently taken into account.
4) Back scattering of gravitational waves by spacetime curvature is neglected as long as the tail terms of radiation is not included.[7]

A priori, point 1) is not distinguished from point 4). However the semi-relativistic approximation naturally distinguishes them. With respect to point 4), the effect of the boundary condition at the event horizon is not included both in the post-Newtonian and semi-relativistic approximations. However, the semi-relativistic approximation can handle point 1) by definition and point 3) because of the identification of the Schwarzschild time coordinate t with the time in the hypothetical flat spacetime. As mentioned several times already, concerning points 2) and 4), semi-relativistic formula is not so appropriate, but it may be possible to solve these issues by introducing phenomenological correction terms. Furthermore, since the semi-relativistic approximation is analogous to the conventional quadrupole approximation, it is possible to introduce a backreaction force in the equations of motion which is consistent with the amount of emitted gravitational waves. Hence it seems meaningful, and perhaps more reasonable than the post-Newtonian approach, to solve such equations of motion with radiation damping, to understand the evolution of a

compact binary in its mildly relativistic phase. If all of these are possible, it will be a fairly simple method compared with the post-Newtonian approach because in the latter, it is very difficult and complicated to include the higher multipole radiation reaction and the tail term of radiation.[7),23)]

We have also estimated the effect of radiation damping on the evolution of the orbit, assuming that the quasi-periodicity of the orbit is maintained. Although our results cannot be applied to the case $\mu=O(1)$, let us tentatively ignore this fact and consider the implication of our results in connection with the work by Lincoln and Will.[6)] They pointed out that the infall velocity, $\dot{r}$, becomes comparable to the orbital velocity, $r\dot{\varphi}$, at $r\sim 8$ for the initially quasi-circular orbit of a system of equal mass particles; $\mu=1/4$, and at $r\sim 5$ for the mass ratio 10 : 1; $\mu=10/121$. If we boldly assume that the radial infall velocity is directly given in terms of the energy loss rate for the circular orbit, we find $\dot{r}=2r^{3/2}(r-3)^{3/2}/\{(r-6)\dot{E}/\mu\}$. Using this crude formula with $\dot{E}$ of the calculated results, the radius at which $\dot{r}/(r\dot{\varphi})=1$ is $r\sim 6.5$ for $\mu=1/4$, and $r\sim 6$ for $\mu=10/121$. Of course these values differ from those calculated by Lincoln and Will. This is because their estimate is based on the post-Newtonian approximation and the relativistic effect is not sufficiently included, while in our estimate, although the general relativistic effect is included, the effect non-linear in μ is not included in a consistent manner.

Apparently, in order to obtain a more reliable estimate of the orbital features in the final phase of coalescence, some improvements are necessary both in the post-Newtonian type approach and in the relativistic test particle type approach. As for the latter, an immediate issue is to find a method to incorporate the radiation reaction consistently in the calculations of the orbit and the gravitational radiation, at least in the lowest order of μ.

In this paper, we have calculated the outgoing gravitational waves induced by a test particle moving around a black hole to investigate the orbital evolution of a binary system. However, when we consider the last stage of the evolution of a binary such as black hole-black hole or black hole-neutron star binary, it is expected that the ingoing waves through the black hole event horizon are not negligible compared with outgoing ones. Therefore we must calculate the ingoing waves as well as the outgoing ones. We plan to do so in a forthcoming paper.

The numerical calculations are mainly performed on a YHP-S720 work station. This work was supported in part by the Grant-in-Aid for Scientific Research on Priority Area of the Ministry of Education (04234104).

Appendix

In this appendix, we summarize the explicit form of $S_{lm\omega}$ in Eq. (2·3). The expression is basically the same as given in Ref. 20), except for its specialization to bound orbits.

Following the formulation of Ref. 21), we express the source term $S_{lm\omega}$ in terms of a new function $W_{lm\omega_n}$ as

$$S_{lm\omega}=\mu\sum_n\frac{2\pi}{\Delta t}\delta(\omega-\omega_n)\frac{r-2}{r^3}e^{-i\omega_n r^*}W_{lm\omega_n} \tag{A·1}$$

or equivalently,

$$\tilde{S}_{lm\omega_n}=\frac{r-2}{r^3}e^{-i\omega_n r^*}W_{lm\omega_n}\,, \tag{A·2}$$

where ω_n is defined in Eq. (2·14). The function $W_{lm\omega_n}$ is given as

$$W_{lm\omega_n}(r)=\frac{1}{r}\left[W_{0\,lm\omega_n}(r)-\int_r^\infty dr'\,W'_{1\,lm\omega_n}(r')+\int_r^\infty dr'\int_{r'}^\infty dr''\,W''_{2\,lm\omega_n}(r'')\right], \tag{A·3}$$

where

$$\begin{aligned}
W_0(r)&=\frac{C_2}{\gamma}\cos(\omega_n t(r)-m\varphi(r))\theta(r_{\max}-r)\theta(r-r_{\min})e^{i\omega_n r^*}\,,\\
W'_1(r)&=\left\{\left(-\frac{2C_2}{r\gamma}-i\frac{2r^2}{\Delta}\frac{\varepsilon}{\gamma}C_1\right)\cos(\omega_n t(r)-m\varphi(r))\right.\\
&\quad\left.-2\frac{r^2}{\Delta}C_1\sin(\omega_n t(r)-m\varphi(r))\right\}e^{i\omega_n r^*}\theta(r_{\max}-r)\theta(r-r_{\min})\,,\\
W''_2(r)&=\left\{\left(-\frac{2C_2}{r^2\gamma}-\frac{r^4}{\Delta^2}\left(\frac{\varepsilon^2}{\gamma}+\gamma\right)C_0\right)\cos(\omega_n t(r)-m\varphi(r))\right.\\
&\quad\left.+2i\frac{r^4}{\Delta^2}\varepsilon C_0\sin(\omega_n t(r)-m\varphi(r))\right\}e^{i\omega_n r^*}\theta(r_{\max}-r)\theta(r-r_{\min})
\end{aligned} \tag{A·4}$$

with $\Delta=r(r-2)$ and $\gamma=|dr/d\tau|$. The three constants C_0, C_1 and C_2 are given by

$$\begin{aligned}
C_0&=\sqrt{\lambda(\lambda+2)}\,{}_0P_{lm}\left(\frac{\pi}{2}\right),\\
C_1&=\sqrt{\lambda}\,L_z\,{}_{-1}P_{lm}\left(\frac{\pi}{2}\right),\\
C_2&=L_z^2\,{}_{-2}P_{lm}\left(\frac{\pi}{2}\right),
\end{aligned} \tag{A·5}$$

where $\lambda=(l-1)(l+2)$ and ${}_sP_{lm}(\theta)$ is defined in terms of the spin weighted spherical harmonics ${}_sY_{lm}(\theta,\varphi)$ as

$${}_sP_{lm}(\theta)={}_sY_{lm}(\theta,0)\,. \tag{A·6}$$

References

1) R. E. Vogt, in *Proceeding of the Sixth Marcel Grossmann Meeting on General Relativity*, ed. H. Sato and T. Nakamura (World Scientific, Singapore, 1992), p. 244.
A. Abramovici et al., Science **256** (1992), 325.
2) A. Brillet, in *Proceeding of International Symposium on Neutrino Astrophysics* (Takayama, Japan, October 1992), to appear.
3) K. Oohara and T. Nakamura, Prog. Theor. Phys. **82** (1989), 535; **83** (1990), 906; **88** (1992), 307.
4) T. Nakamura and K. Oohara, Prog. Theor. Phys. **82** (1989), 1006; **86** (1991), 73.

5) M. Shibata, T. Nakamura and K. Oohara, Prog. Theor. Phys. **88** (1992), 1079; **89** (1993), 809.
6) C. W. Lincoln and C. M. Will, Phys. Rev. **D42** (1990), 1123.
7) A. G. Wiseman, Phys. Rev. **D46** (1992), 1517.
8) L. E. Kidder, C. M. Will and A. G. Wiseman, Class. Quantum. Grav. **9** (1992), L125.
9) C. Cutler et al., Phys. Rev. **D47** (1993), 1511; Caltech Preprint GRP-316.
10) T. Nakamura, K. Oohara and Y. Kojima, Prog. Theor. Phys. Suppl. No. 90 (1987), Part II.
11) J. H. Taylor and J. M. Weisberg, Astrophy. J. **345** (1989), 434.
12) A. Wolszczan, Nature **350** (1991), 688.
13) S. B. Anderson et al., Nature **346** (1990), 42.
14) L. Smarr, in *Source of Gravitational Radiation,* ed. L. Smarr (Cambridge University Press, Cambridge, 1979), p. 245.
15) M. Davis, R. Ruffini, W. H. Press and R. H. Price, Phys. Rev. Lett. **27** (1971), 1466.
M. Davis, R. Ruffini and J. Tiomno, Phys Rev. **D5** (1972), 2932.
16) R. F. Stark and T. Piran, Phys. Rev. Lett. **55** (1985), 891.
17) S. L. Detweiler, Astrophys. J. **225** (1978), 687.
18) K. Oohara and T. Nakamura, Phys. Lett. **94A** (1983), 349; Prog. Theor. Phys. **70** (1983), 757.
19) K. Oohara and T. Nakamura, Prog, Theor. Phys. **71** (1984), 91.
20) K. Oohara, Prog. Theor. Phys. **71** (1984), 738.
21) M. Sasaki and T. Nakamura, Phys. Lett. **87A** (1981), 85.
22) R. Ruffini and M. Sasaki, Prog. Theor. Phys. **66** (1981), 1627.
M. Sasaki, Prog. Theor. Phys. **69** (1983), 815.
23) L. Blanchet and T. Damour, Phys. Rev. **D37** (1988), 1410.